nature portfolio

https://doi.org/10.1038/s41893-021-00831-2

Supplementary information

Sustainable high-strength macrofibres extracted from natural bamboo

In the format provided by the authors and unedited

Supplementary Information for

Sustainable high-strength macrofibers extracted from natural bamboo

Zhihan Li[1,‡], Chaoji Chen[1,‡], Hua Xie[1,‡], Yuan Yao[2], Xin Zhang[1], Alexandra Brozena[1], Jianguo Li[1], Yu Ding[1], Xinpeng Zhao[1], Min Hong[1], Haiyu Qiao[1], Lee M. Smith[3], Xuejun Pan[4], Robert Briber[1], Sheldon Q. Shi[3], Liangbing Hu[1,5]*

1. Department of Materials Science and Engineering, University of Maryland, College Park, MD, USA
2. Yale School of the Environmental, Yale University, New Haven, CT, USA
3. Department of Mechanical and Energy Engineering, University of North Texas, Denton, TX, USA
4. Department of Biological Systems Engineering, University of Wisconsin-Madison, Madison, WI, USA
5. Center for Materials Innovation, University of Maryland, College Park, MD, USA.

This supplementary information file includes:

• Supplementary Notes 1–3

• Supplementary Figures 1–17

• Supplementary Tables 1–7

• Supplementary Video 1–2

• Supplementary References 1–71

Supplementary Note 1: Structural characterization by high-resolution X-ray scattering

Wide angle X-ray scattering (WAXS) is a well-established method for determining the microfibril angle (MFA), which describes the angle between the cellulose microfibrils and the longitudinal axis of the bamboo macrofiber[1]. WAXS can also be used to determine the crystallinity of the bamboo macrofiber and the average size of its cellulose crystallites, in which the (200) reflections correspond to the inter-sheet spacing of the cellulose Iβ crystals.

Using the symmetrical transmission mode of the diffraction pattern, the angular range was reduced from 360° to 180° by summing the halves consisting of the angular ranges 1–180° and 181–360°. The resulting azimuthal intensity distribution profiles of the cellulose crystal reflections at (200) along the arc of the 2D WAXS pattern of the bamboo macrofiber was used to calculate the microfibril orientation index (f_c) according to the equations[1]:

$$f_c = \frac{180^\circ - \mathrm{FWHM}}{180^\circ} \quad (1)$$

in which FWHM is the full width of the half-maximum of the azimuthal profiles from the selected equatorial reflection.

The calculation of MFA is done by curve fitting using the Nedler Mead least square routine according to Alain Bourmaud's method[2]. The theoretical function considered includes two Gaussian curves and a baseline (a constant value):

$$y = A_0 + A_1 \exp\left(-\frac{(x-m_1)^2}{\sigma_1}\right) + A_2 \exp\left(-\frac{(x-m_2)^2}{\sigma_2}\right) \quad (2)$$

The MFA is then deduced from the parameters of the fitted function according to Cave's equation[3]:

$$MFA = 0.6\,T \quad (3)$$

$$T = \sigma_1 + \sigma_2 \quad (4)$$

The crystallinity index (*CI*) of macrofibers is calculated as the ratio of the integrated intensity of the crystalline peaks to the sum of the crystalline and amorphous intensities[4]:

$$CI = \frac{I_{crystalline}}{I_{crystalline} + I_{amorphous}} \quad (5)$$

in which $I_{crystalline}$ is the total area of the crystalline cellulose, and $I_{amorphous}$ is the area of the amorphous cellulose. In this work, the amorphous and crystalline areas were extracted by the Gaussian curve-fitting process from the diffraction intensity profiles of cellulose crystal reflections in the WAXS patterns of the macrofibers.

In our work, the strong (200) cellulose reflection is well suited to the Scherrer equation as the (200) reflection has a single and clear direction that corresponds to the lateral dimension of the microfibril. The FWHM of the (200) reflection was used to calculate the average size of the cellulose crystallites. The average size of the crystallites was estimated from the widths of the reflections using the Scherrer formula[5]:

$$B_{hkl} = \frac{K\lambda}{\zeta \cos(\varphi)} \quad (6)$$

in which B_{hkl} is the crystallite size in the direction perpendicular to the lattice planes, K is a numerical factor frequently referred to as the crystallite-shape factor, λ is the wavelength of the X-rays, φ is the Bragg angle, and ξ is the full width half maximum in radians. The effect of instrumental broadening on the width of the reflections was included by assuming that the shapes of both the reflection and the instrumental function were approximately Gaussian, and the value of ξ was calculated using the formula:

$$\zeta = \sqrt{(b_s^2 - b_i^2)} \quad (7)$$

in which b_s is the FWHM of the reflection (200), and b_i is the instrumental broadening.

The average *d*-spacing of the crystalline planes were measured by XRD and calculated using Bragg's formula[6]:

$$d = \frac{n\lambda}{2\sin\varphi} \quad (8)$$

in which φ is the angle between the planes and the incoming X-rays, n is an integer, and λ is the incident wavelength.

Supplementary Note 2: Weibull distribution

In our work, taking the volume (V), diameter (D) and length (L) of the macrofibers into consideration ($V = L\pi D^2/4$), the failure probability of the bamboo cellulose macrofibers and applied strength σ is given by the improved Weibull statistical modeling as following

$$F = 1 - exp\left\{-\left(\frac{V}{V_0}\right)^{\beta}\left(\frac{\sigma}{\sigma_0}\right)^{m}\right\} \quad (9)$$

where F is the failure probability of the fiber with V at a stress less than or equal to σ. L_0 and D_0 are reference length and diameter, respectively. β is a measure sensitivity to the fiber volume, σ_0 is the characteristic stress, and m is the Weibull modulus describing the variability of the dispersion in fiber strengths. Since all the bamboo microfibers measured in this work have the same length, Eq. (9) can be simplified as,

$$F = 1 - exp\left\{ -\left(\frac{D}{D_0} \right)^{2\beta} \left(\frac{\sigma}{\sigma_0} \right)^{m} \right\} \qquad (10)$$

Supplementary Note 3: Life cycle carbon analysis for bamboo cellulose macrofibers

The life cycle inventory (LCI) of preparing bamboo cellulose macrofibers are documented in Table 5. The system boundary is cradle-to-gate, including the extraction of raw materials, transportation, and production. The LCI data of the upstream production of chemicals, electricity, and deionized water were modeled based on the data collected from the Ecoinvent 3.5 database[7]. Specifically, peroxyformic acid solution used in Step 2 was prepared using formic acid, hydrogen peroxide, sulfuric acid, and deionized water (Table 5). The LCI of formic acid upstream production were modeled based on the butane oxidation process in the United States[8]. The LCI of hydrogen peroxide production were modeled based on the anthraquinone process, the primary industrial process for hydrogen peroxide production[9]. The LCI of sulfuric acid production were modeled based on the contact process, the dominate process to produce sulfuric acid in the United States[10]. The LCI of sodium hydroxide (used in Step 3 in Table 5) upstream production was modeled based on the chlor-alkali electrolysis using diaphragm cell, the dominant process in the North America[11]. The LCI of U.S. electricity mixes were used for the electricity used in bamboo cellulose macrofibers preparation and all upstream production of chemicals. The greenhouse gas (GHG) emission generated from the cultivation and harvest of bamboo is set to be 0.0156 kg CO_2/kg of bamboo[12]. Chemicals were assumed to be transported from chemical suppliers by trucks at a distance of 352 km based on the average distances of truck transportation for basic chemicals in the United States in 2017[13]. The bamboo was assumed to be transported by trucks at a distance of 222 km based on the average distances of truck transportation for logs and other wood in rough in the United States in 2017[13]. The truck was assumed to be diesel-powered combination truck, and the LCI data of transportation and upstream production of fuels was collected from the USLCI (U.S. Life Cycle Inventory) database[14]. The carbon footprint is reported in CO_2e using 100-year global warming potential conversion factors reported by the Intergovernmental Panel on Climate Change for none-CO_2 greenhouse gases[15]. The carbon sequestration of bamboo was estimated based on the carbon content of bamboo (0.5 kgC/kg bamboo)[12,16] and the molecular weight of carbon (12 g/mol) and carbon dioxide (44 g/mol).

Through this cradle-to-gate carbon analysis, the carbon footprint of the bamboo cellulose macrofibers on a 1 kg basis was calculated. However, to compare this result with other materials, additional normalization that considers material properties is needed. For a high-strength material, less mass will be needed to meet a particular strength requirement for composites or other applications. If σ_b is the tensile strength of the bamboo cellulose macrofiber, σ_s is the tensile strength of the substitute material, and A_b and A_s are the cross-sectional areas for the

bamboo cellulose macrofibers and substitute material used in the same application (e.g., a composite), then

$$\sigma_{\mathrm{b}} = \frac{F}{A_{\mathrm{b}}} \quad (11)$$

$$\sigma_{\mathrm{s}} = \frac{F}{A_{\mathrm{s}}} \quad (12)$$

The force F in the two equations should be equal for materials that can provide the same strength. Therefore, we can obtain:

$$\frac{\sigma_{\mathrm{b}}}{\sigma_{\mathrm{s}}} = \frac{A_{\mathrm{s}}}{A_{\mathrm{b}}} \quad (13)$$

For two materials used in the same application, the length/height (l) should be the same, thus the ratio of σ_b to σ_s can be expressed as:

$$\frac{\sigma_{\mathrm{b}}}{\sigma_{\mathrm{s}}} = \frac{A_{\mathrm{s}} l}{A_{\mathrm{b}} l} = \frac{V_{\mathrm{s}}}{V_b} = \frac{\rho_b}{\rho_s} \times \frac{M_s}{M_b} \quad (14)$$

in which ρ_b and ρ_s are the density of the bamboo cellulose macrofiber and substitute material, respectively. The mass ratio of the two materials (to satisfy the same strength requirement) can be derived as:

$$\frac{M_{\mathrm{s}}}{M_b} = \frac{\sigma_{\mathrm{b}}}{\sigma_{\mathrm{s}}} \times \frac{\rho_{\mathrm{s}}}{\rho_b} \quad (15)$$

Thus the carbon footprint results can be normalized based on the mass ratio and carbon intensity (kg CO_2e/kg of material) of the bamboo cellulose macrofibers and substitute materials. The mass reduction percentage enabled by replacing one substitute material with bamboo cellulose macrofibers can be calculated as 1 minus the mass ratio (the mass ratio results are shown in Fig. 5a).

$$\frac{GHGI_{\mathrm{b}} M_b}{GHGI_{\mathrm{s}} M_s} = \frac{GHGI_{\mathrm{b}}}{GHGI_{\mathrm{s}}} \times \frac{\sigma_{\mathrm{s}}}{\sigma_{\mathrm{b}}} \times \frac{\rho_{\mathrm{b}}}{\rho_s} \quad (16)$$

In this study, several commonly used fiber materials were chosen as the substitute materials. Their carbon intensity and strength data were collected from literature and shown in Supplementary Table 6.

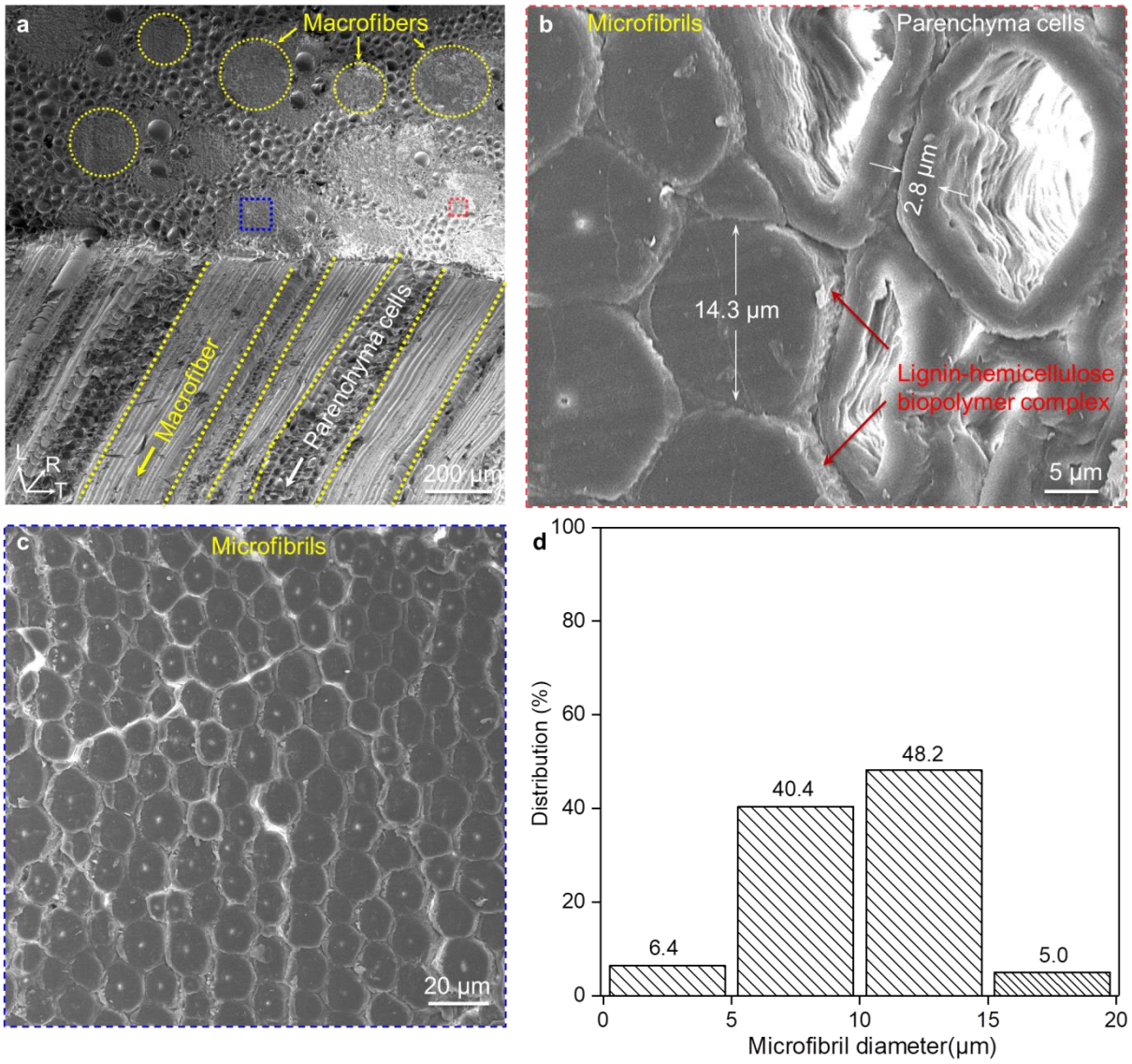

Supplementary Fig. 1 | a, SEM image of unidirectional macrofibers homogeneously embedded in the parenchyma cells of the bamboo stem wall. **b,** Magnified SEM image showing the rigid macrofibers and soft parenchymal cells are connected via a lignin-hemicelluloses biopolymer complex. **c,** Magnified SEM image showing a typical macrofiber, which consists of hundreds of solid and densely aggregated microfibrils. **d,** The microfibrils in a typical macrofiber have an average diameter of ~13 μm and high aspect ratio of ~200.

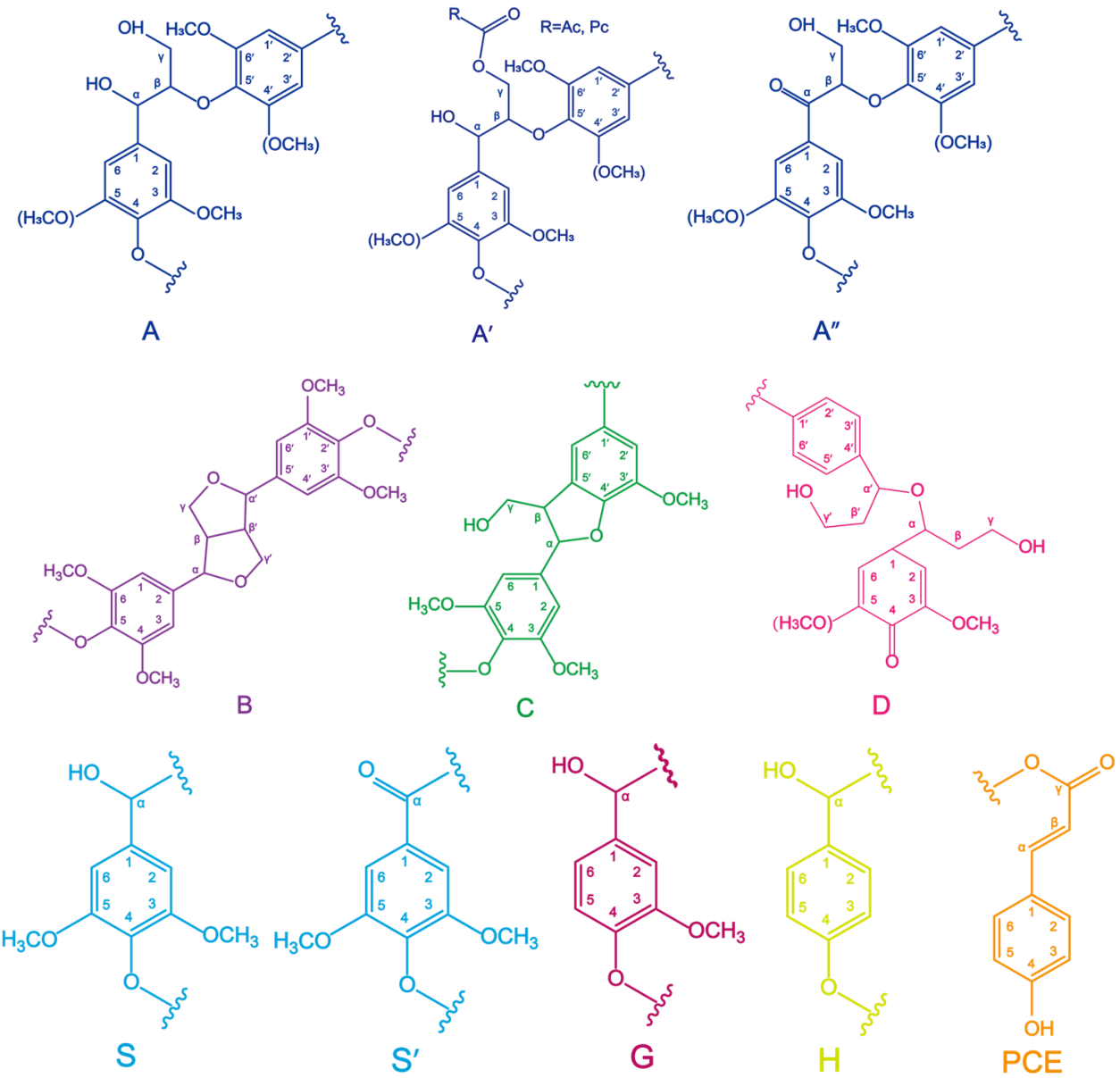

Supplementary Fig. 2 | The main classical structures found in lignin: (A) β-O-4′ linkages; (A′) acylated β-O-4′ substructures (R = Ac, *p*-CA); (A″) C_α-oxidized β-O-4′ linkage substructures; (B) resinol structures formed by β-β′, α-O-γ′ and γ-O-α′ linkages; (C) phenylcoumarane structures formed by β-5′ and α-O-4′ linkages; (D) spirodienone structures formed by β-1′ linkages; (S) syringyl unit; (S′) oxidized syringyl unit linked to a carbonyl or carboxyl group at C_α (phenolic); (G) guaiacyl unit; (H) *p*-hydroxyphenyl units; (*p*-CE) *p*-coumarates units.

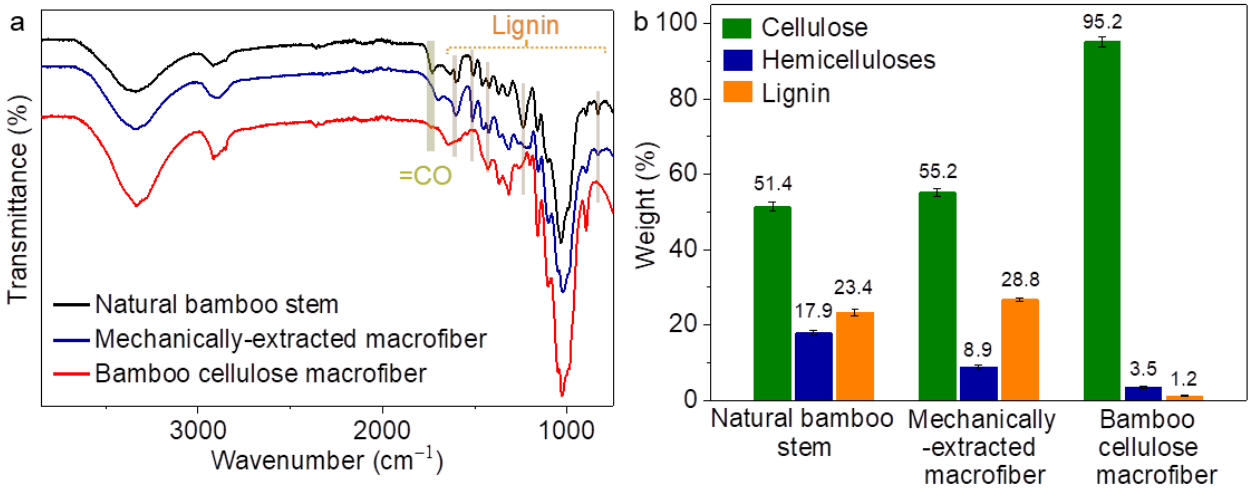

Supplementary Fig. 3 | a, FTIR spectra of natural bamboo stem, mechanically-extracted macrofibers, and the bamboo cellulose macrofibers isolated via the selective delignification process. After the first chemical delignification step, the absorption peaks of hemicelluloses at 1740 cm^{-1} (=CO stretching vibration of the carboxylic acid and ester groups) and lignin at 1594 and 1508 cm^{-1} (C=C stretching vibration), 1457 cm^{-1} (CH_2 deformation stretching), 1238 cm^{-1} (C–O vibration in the syringyl ring), and 835 cm^{-1} (C-H aromatic bending) disappear in the spectra of bamboo cellulose macrofibers, indicating the effective elimination of lignin and hemicelluloses from the material. **b,** The cellulose, hemicelluloses, and lignin contents in natural bamboo stem, mechanically-extracted macrofibers, and bamboo cellulose macrofibers. The relative cellulose content of the bamboo cellulose macrofibers increases substantially (up to 95%) after the delignification treatment of the bamboo stem starting material. The cellulose and lignin content are stable in mechanically-extracted macrofibers while the hemicelluloses are prone to thermally degrade during the high temperature hydrothermal treatment.

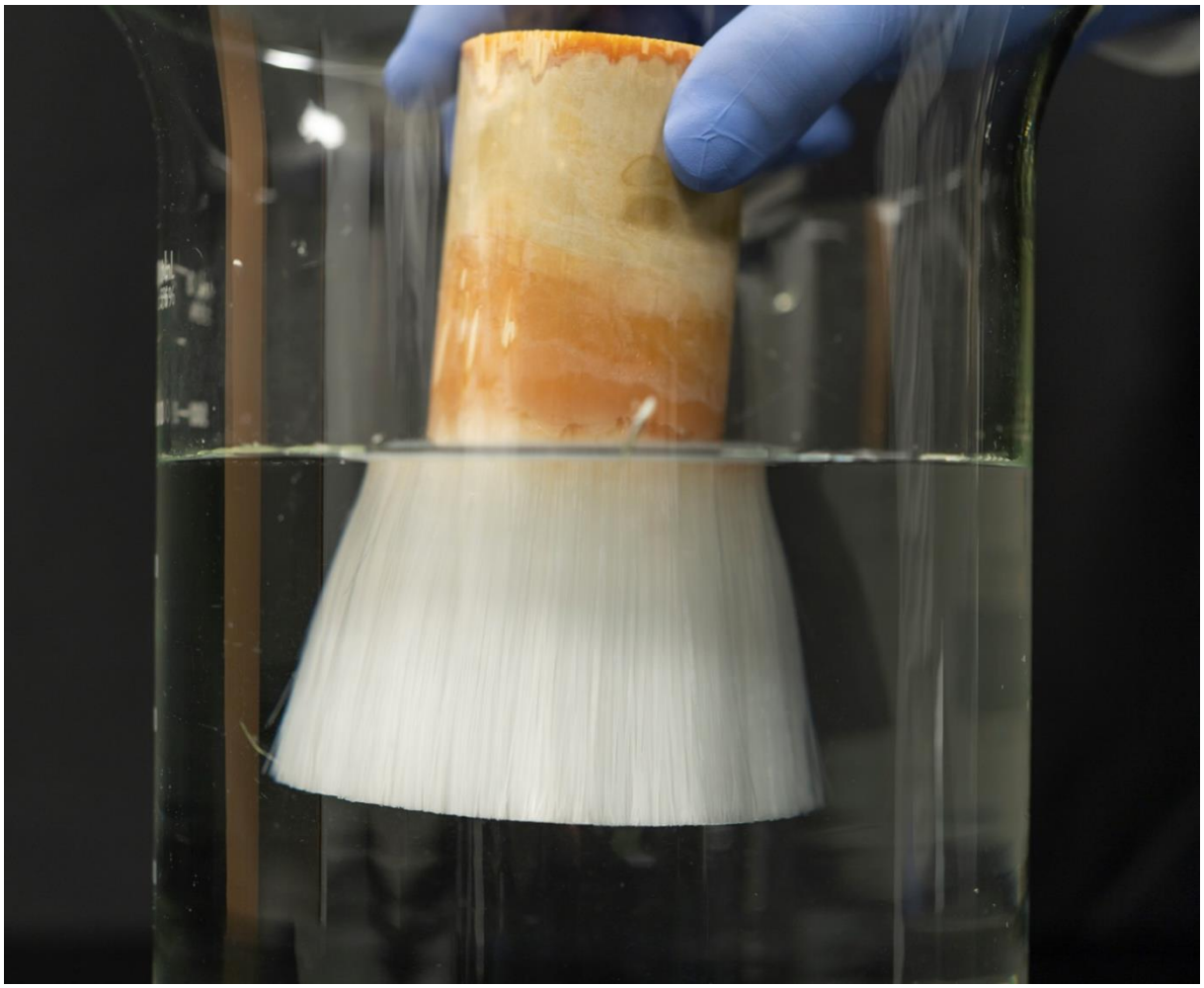

Supplementary Fig. 4 | Photograph of the completely delignified bamboo stem during the washing process. After treatment, the bamboo separates into distinct fibers.

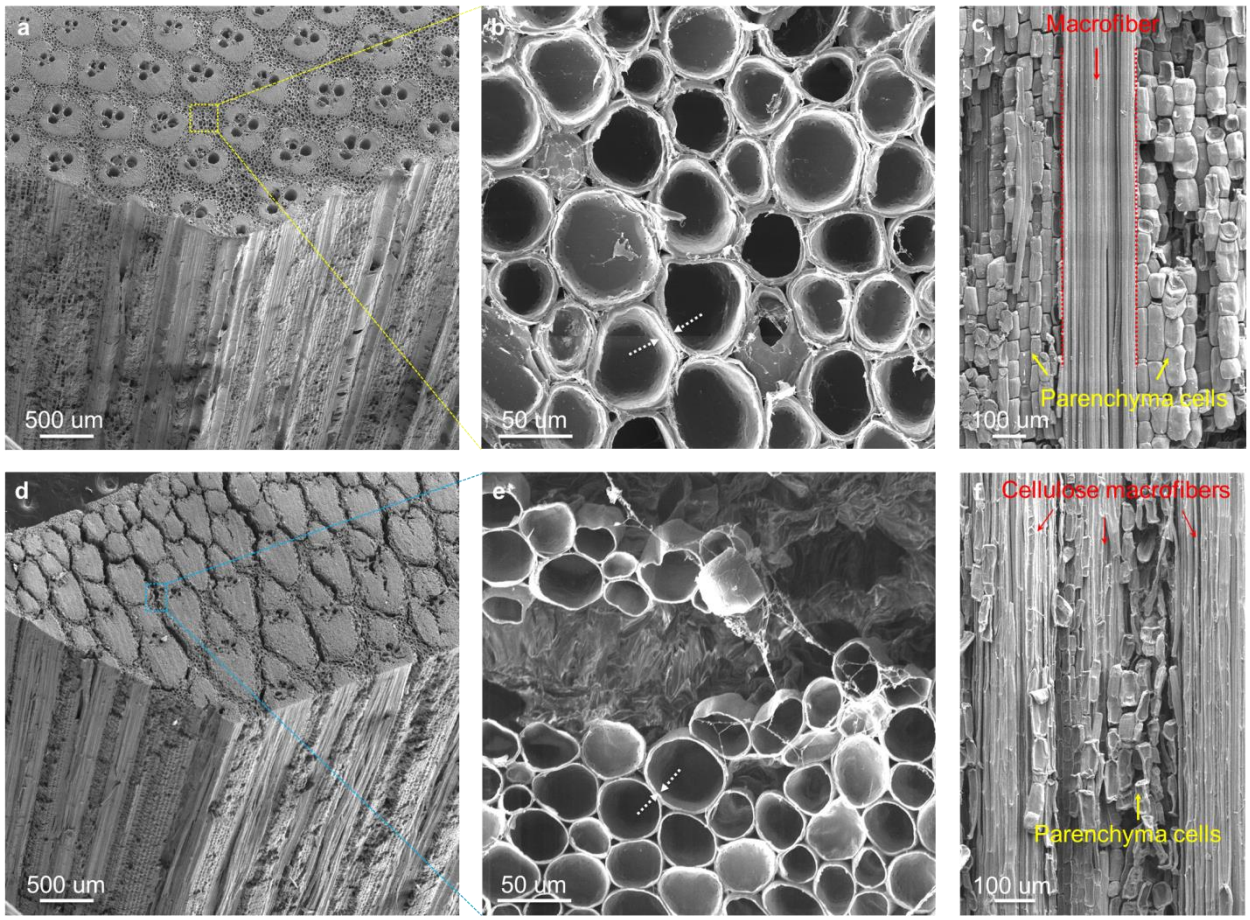

Supplementary Fig. 5 |. **a,** SEM image of the natural bamboo stem wall. **b,** Magnified SEM image showing the hollow parenchyma cells are connected by high concentrations of lignin at the cell interfaces. **c,** A side-view SEM image showing the parenchyma cells distributed around the macrofibers in the natural bamboo stem. **d,** A SEM image of the partially delignified bamboo stem shows cracks that appear in the parenchyma cell region, as well as a loose connective structure between the parenchyma cells and adjacent macrofibers compared to the unmodified natural bamboo. **e,** A magnified SEM image showing the parenchyma cells, which detach from neighboring cells during the delignification process and feature a decreased cell wall thickness. **f,** A side-view SEM image showing how the parenchyma cells naturally fall away from the cellulose macrofiber surface after the removal of the lignin binder by the delignification process.

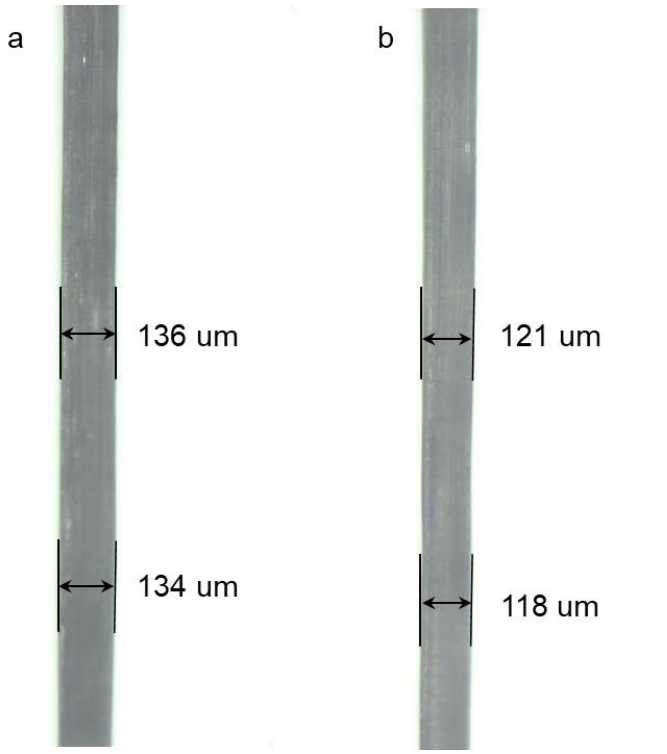

Supplementary Fig. 6 | Optical microscopy images of typical delignified bamboo macrofiber **a**, before and **b**, after the air-drying process. We observed ~10-12% shrinkage across the diameter change of 50 bamboo cellulose macrofibers.

Supplementary Fig. 7 | Photograph of delignified bamboo stems demonstrating different lengths of cellulose macrofibers that can be obtained simply by immersing more of the bamboo stem in the delignification solution.

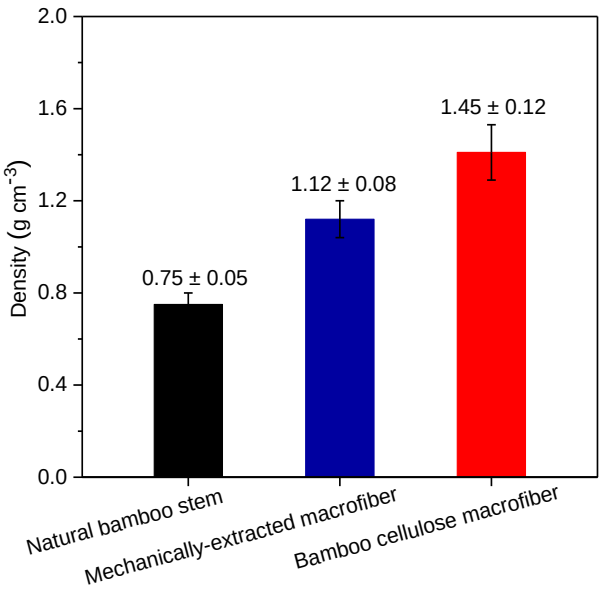

Supplementary Fig. 8 | The densities of the natural bamboo stem, mechanically-extracted macrofibers, and bamboo cellulose macrofibers.

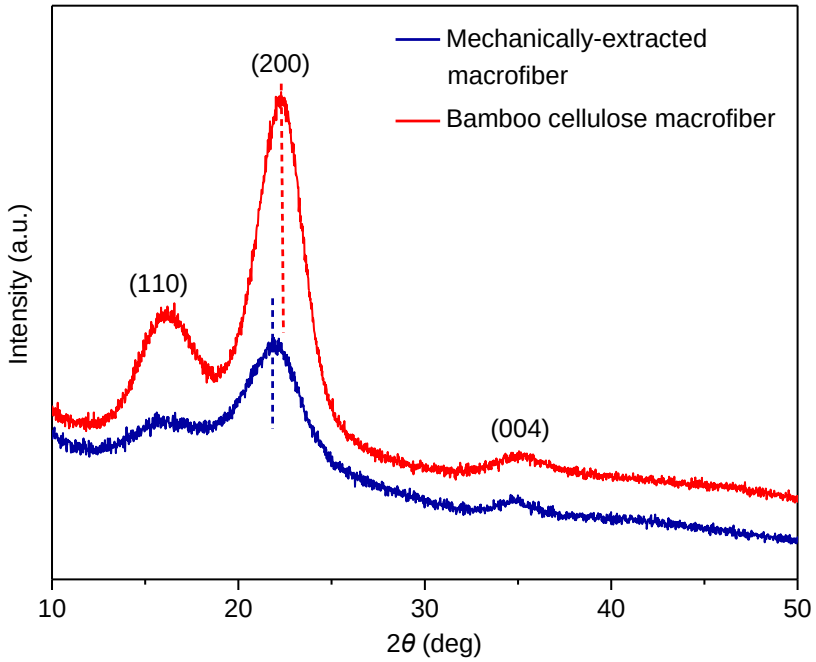

Supplementary Fig. 9 | The XRD diffraction patterns of the mechanically-extracted macrofibers and bamboo cellulose macrofibers, the latter of which displays a blueshift of 0.55^{o} in the (200) peak. Using Bragg's formula, we found the bamboo cellulose macrofibers feature a decrease of 0.06 Å in the average distance between the (200) crystal planes compared to the mechanically-extracted control.

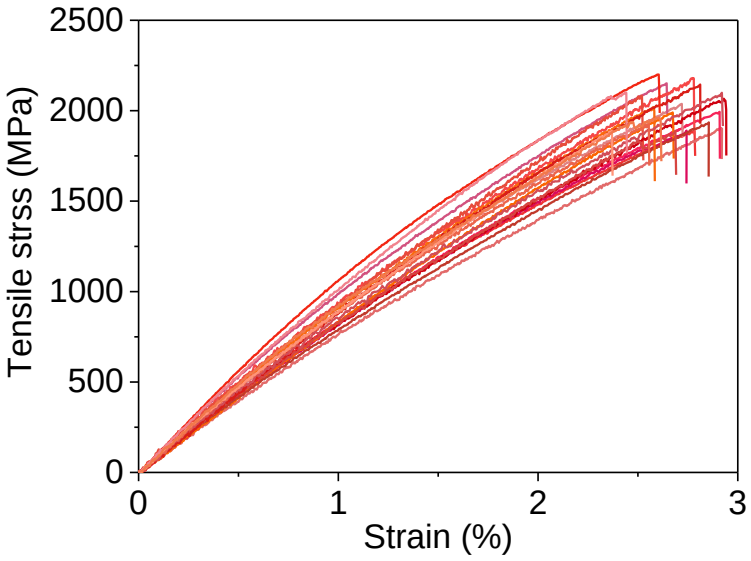

Supplementary Fig. 10 | The similar stress-strain curves of bamboo cellulose macrofibers with a gauge length of 1 cm indicated the consistent tensile properties of the fibers.

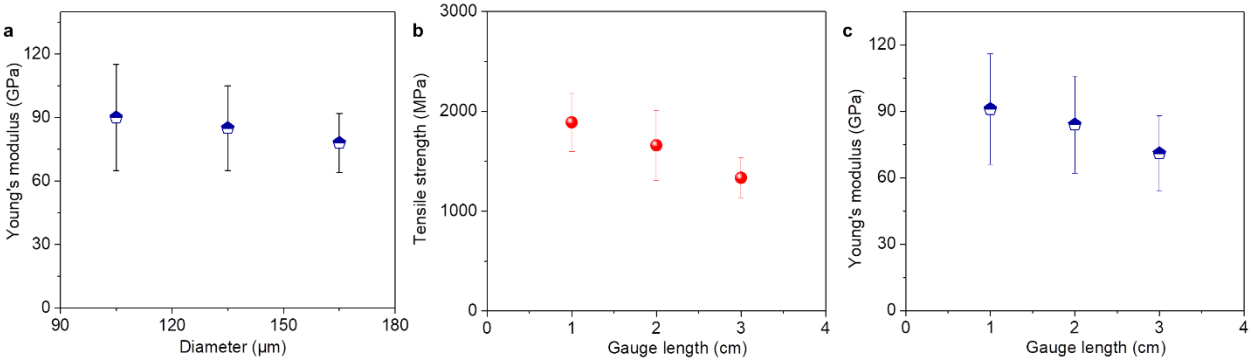

Supplementary Fig. 11 | a, The Young's modulus of bamboo cellulose macrofibers of different diameter. **b,** The tensile strength and **c,** Young's modulus of bamboo cellulose macrofibers of different gauge length.

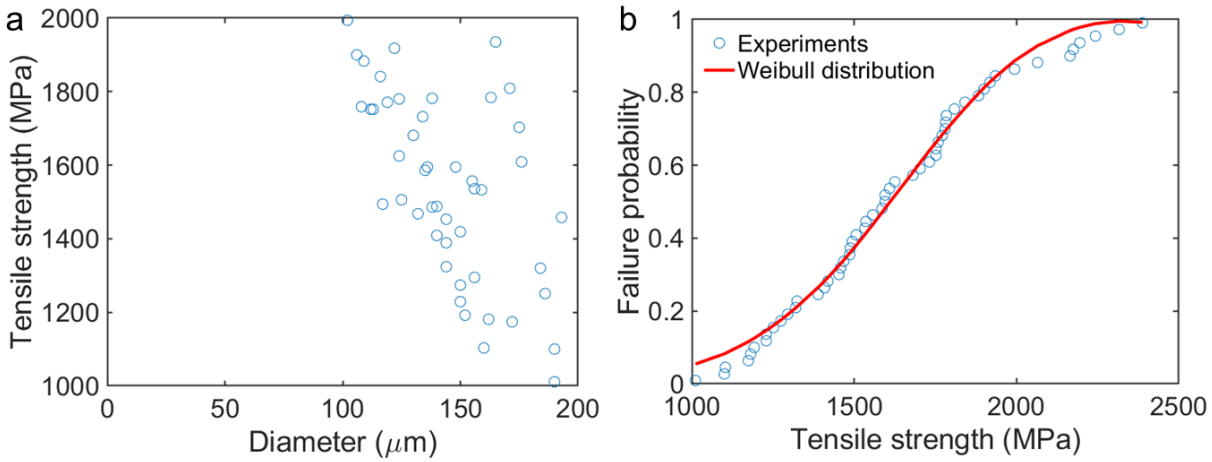

Supplementary Fig. 12 | a, Relationship between the tensile strength and diameter of bamboo cellulose macrofibers. **b,** The cumulative Weibull probability distributions for the bamboo cellulose macrofibers.

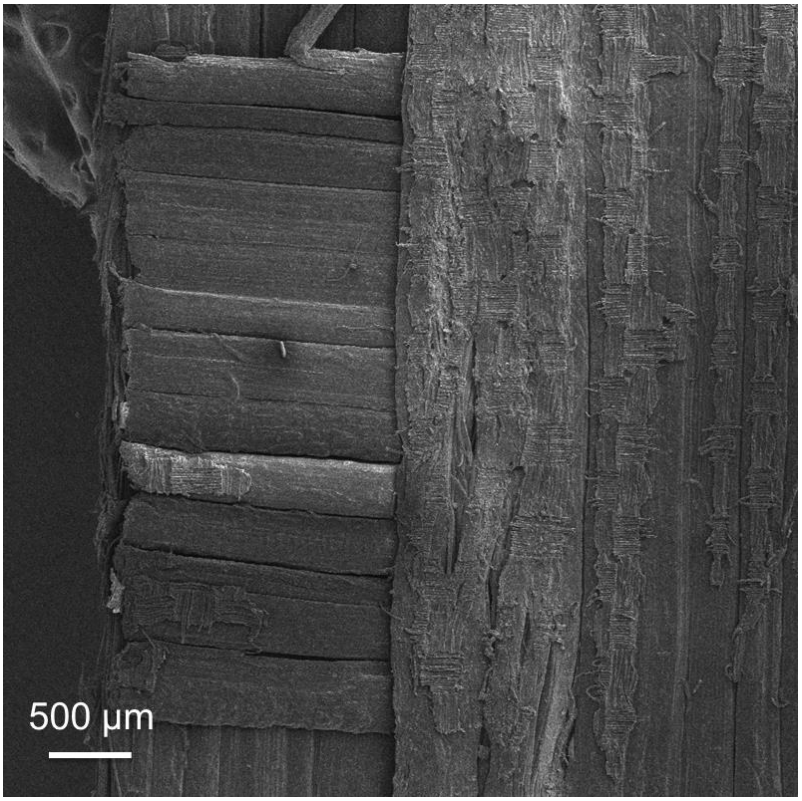

Supplementary Fig. 13 | SEM image showing the bamboo cellulose macrofibers were arranged in an orthogonal, interlacing pattern featuring an aligned structure, in which the fibers did not intertwine.

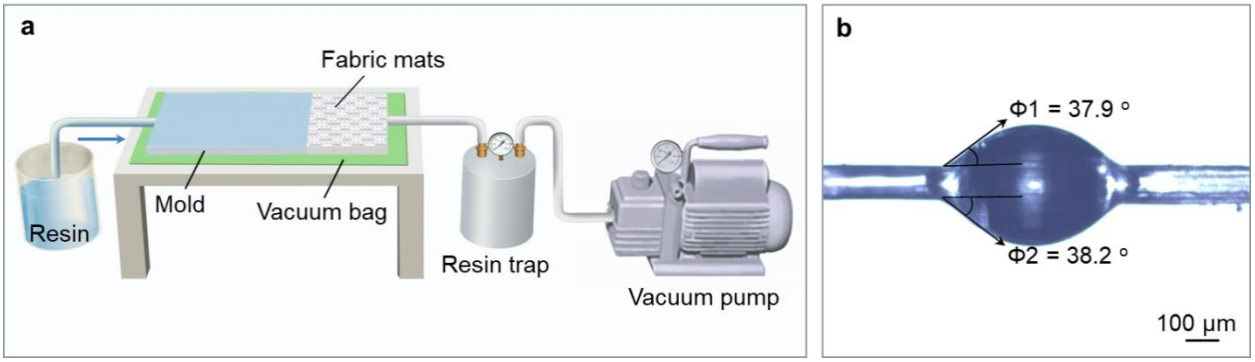

Supplementary Fig. 14 | a, Schematic illustration of the experimental VARTM setup. Multiple layers of bamboo cellulose macrofiber mats were placed in a single-sided mold and impregnated with liquid epoxy resin via vacuum pressure, then cured at 150 ^{o}C with an external pressurization of 13 MPa to produce the fiber/epoxy resin composite. **b**, The contact angle measurement was carried out by directly depositing an epoxy resin micro-drop on the surface of a single bamboo cellulose macrofiber. A contact angle of ~38^{o} was observed, indicating the resin's good wettability and compatibility on the bamboo cellulose macrofibers.

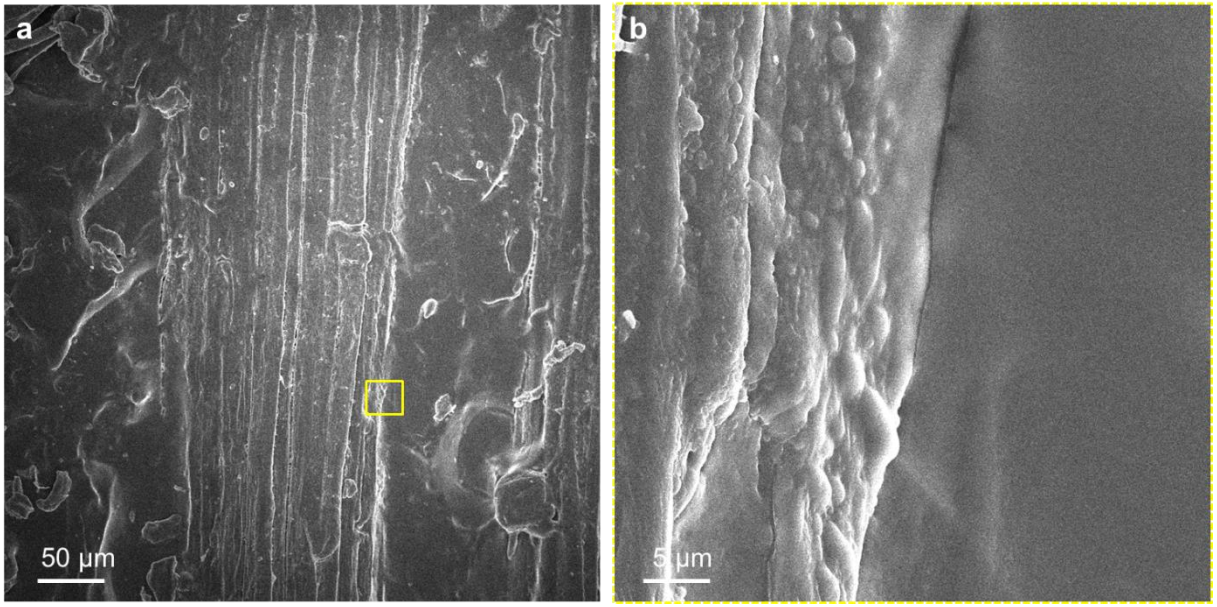

Supplementary Fig. 15 | a, SEM image of the bamboo cellulose macrofibers encapsulated by the epoxy, demonstrating the materials' good interfacial compatibility. **b**, Magnified SEM image showing the bamboo cellulose macrofiber provides good interfacial adhesion with the epoxy matrix.

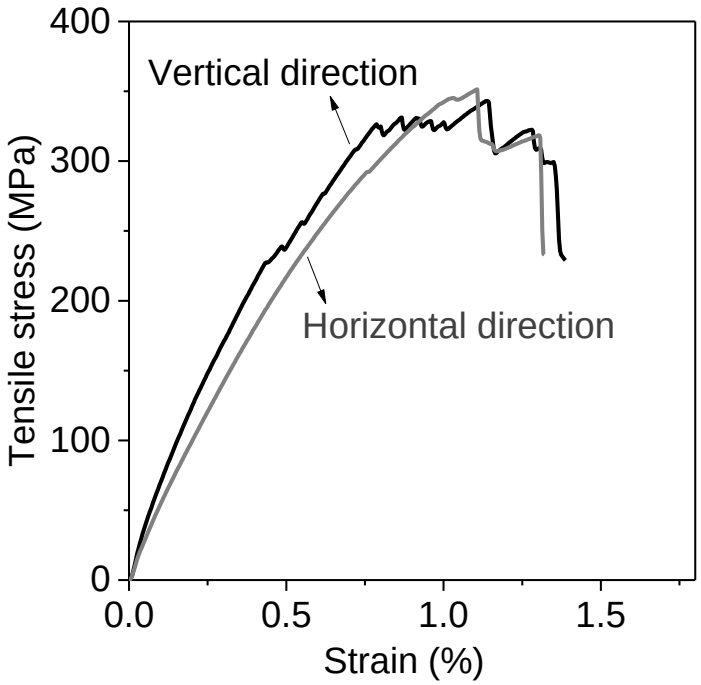

Supplementary Fig. 16 | Typical tensile stress–strain curves of the BFRC tested along the horizontal and vertical directions of the composite (relative to the fiber orientations), both of which feature almost the same tensile strength of ~350 MPa.

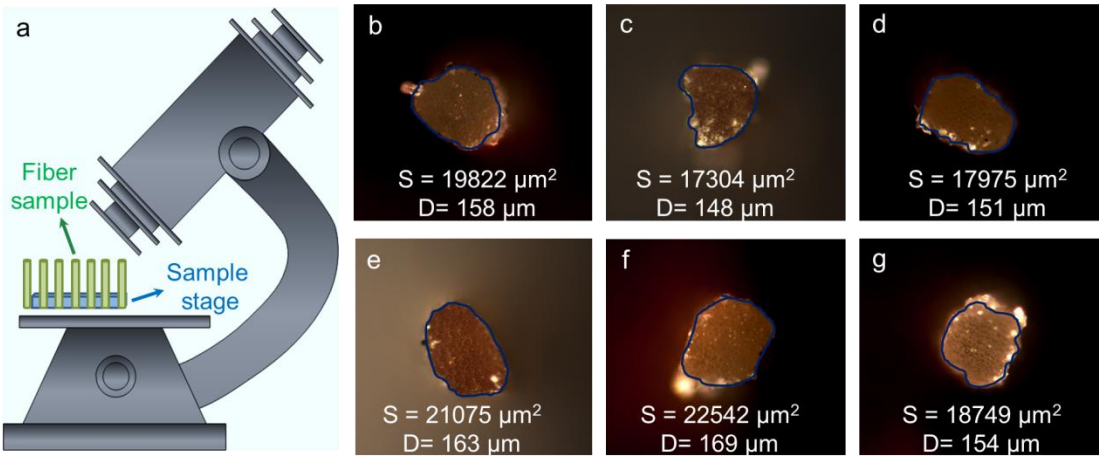

Supplementary Fig. 17 | a, Schematic of cross-sectional area measurement of macrofiber. **b-g,** Typical cross-section and the equivalent diameter determination of the testing macrofibers.

Supplementary Table 1 | Comparison of the lignin content and mechanical properties of our long bamboo cellulose macrofibers and other reported long bamboo macrofibers obtained from different extraction methods.

Extraction method	Extraction procedure	Lignin removal	Density (g cm^{-3})	Strength (MPa)	Modulus (GPa)	Ref.
Mechanical extraction	-	-	1.40	800	43	[17]
Steam explosion	Bamboo strips were heated at170 ℃ with high pressure (0.8 MPa) in an autoclave for 1h, and steam was immediately released for 5 min, repeat nine times, collected via a sifter machine with mesh filtrating.	4.5%	0.80	441	35.9	[18]
Crushing	Bamboo strips were crushed into small pieces by a roller crusher and boiled at 90 ℃ for 10 h.	No	0.93	250 - 590	22.2 - 54.2	[19]
Retting	Bamboo strips were wetted in water for more than 3 days, beaten, scraped with a knife and combed.	No	0.91	503	35.9	[20]
Steam & rolling	Bamboo culms were pre-treated by saturated steam at a pressure of 10 atm (180 ℃) in a pressure tank for 0.5 h and rub-twisted by multi-rollers.	No	1.0	653 - 766	22.5 - 26.7	[21]
Alkali & press	Bamboo strips were treated with 1.5 mol/L NaOH solution at 70℃ for 5 h, and separated by press machine.	8.0%	1.29	473 - 717	33.3 - 43.3	[19] [22] [23]
Compression moulding technique	Bamboo strips were treated with 0.1 mol/L NaOH solution for 72 h, pressed by two flat platens with a constant load of 10 tons.	-	0.9	300 - 1000	-	[24]
Roller mill technique	Bamboo strips were treated with 0.1 mol/L NaOH solution for 72 h, separated by two rolls.	-	0.8	300 - 700	-	[24]
Our Method: Chemical delignification & water-assisted separation	Bamboo culms were treated with 10% peroxyacetic acid solution for 12h to completely removing lignin and hemicelluloses, and separated by water.	94.8%	~1.45	1580 - 2220	61.6 - 120	Our work

Note: "-" indicates no related data was mentioned.

Supplementary Table 2 | The structural parameters of the mechanically-extracted macrofibers and chemically-isolated bamboo cellulose macrofibers.

Macrofiber sample	MFA(^{o})	Orientation index	Crystallite width (Å)	Crystallite spacing d_{200} (Å)	CI%
Mechanically-extracted macrofibers	9.3	0.91	3.4	2.08	42.4
Bamboo cellulose macrofibers	7.2	0.93	3.2	2.02	64.9

Supplementary Table 3 | The relative content of hydrogen bonds and free OH in the natural bamboo stem, mechanically-extracted macrofibers, and chemically-extracted cellulose macrofibers.

Sample	Peak 1 O(6)H···O(3′)		Peak 2 O(3)H···O(5)		Peak 3 O(2)H···O(6)		Peak 4 Free OH(2)		Peak 5 Free OH(6)	
	Peak position	Area ratio	Peak position	Area ratio	Peak position	Area ratio	Peak position	Area ratio	Peak position	Area ratio
Natural bamboo stem	3271	14.0	3340	17.5	3433	23.3	3556	23.5	3589	21.6
Mechanically-extracted macrofibers	3274	16.4	3339	23.0	3434	24.7	3552	19.9	3584	15.8
Chemically-extracted cellulose macrofibers (Bamboo cellulose macrofibers)	3271	19.5	3337	25.8	3423	26.2	3570	16.6	3597	11.7

Supplementary Table 4 | The microfibril angle (MFA) and tensile strength of macrofibers derived from various natural species.

Species	Tensile strength (MPa)	MFA (deg)	Ref.
Hemp	750	6.2	[25]
Wheat straw	300	17	[26]
Coir	250	43~45	[27]
Rhectophyllum camerunense	550	~40	[28]
Soybean straw	200~300	12~14	[29]
Windmill palm	180	38~42	[30]
Flax	300~2100	8.3~9.6	[31]
Jacitara palm	70~120	9~19	[31]
Prosopis juliflora bark	560	10~15	[32]
Rattan	400~600	15~20	[33]
Lygeum spartum L	250	10~14	[34]
Pineapple leaf	630~1300	5~7	[35]
Aloe vera cactus	600	11	[36]
Ramie	600	7.5	[37]
Luffa	80	36~50	[38]
Heteropogon Contortus	500	14	[39]
Tridax procumbens	500	13	[40]
Red banana peduncle	450	12	[41]
Guaruman	600	8	[42]
Mechanically-extracted bamboo macrofiber	350~760	9.3	Our work
Bamboo cellulose macrofiber	1580~2220	7.2	Our work

Supplementary Table 5 | Input and output (life cycle inventory) of the bamboo treatment method presented in this work for the life cycle carbon analysis.

Input/Output	Quantity	Unit
Step 1: Bamboo stem pre-treatment		
Input		
Energy	0.20	kWh
Water	0.34	kg
Bamboo	165-172	g
Output*		
Pre-treated bamboo	162-170	g
Step 2: Treat bamboo stem with peroxyformic acid solution		
Input		
Energy	0.51	kWh
Bamboo	162-170	g
Peroxyformic acid solution was prepared using the following chemicals (see Supplementary Note 3 for details)		
Formic acid (AR >99%)	0.053	kg
Hydrogen peroxide (AR ~30%)	0.142	kg
Sulfuric acid (AR >99.5%)	0.001	kg
Deionized water	0.60	kg
Output*		
Treated bamboo	127-133	g
Step 3: Treat bamboo stem with sodium hydroxide solution and wash in deionized water		
Input		
Bamboo	127-133	g
NaOH 0.5 wt%	0.2	kg
Deionized water	0.40	kg
Output		
Bamboo	60 -70	g
Wastewater	0.6	kg
Bio-waste (parenchymal cells removed from bamboo)	65 - 67	g

*The output of Steps 1 and 2 only includes bamboo, as the remaining solution was reused.

Supplementary Table 6 | Density, tensile strength, and carbon intensity (cradle-to-gate) of substitute materials and bamboo cellulose macrofibers

Materials	Density (g/cm^3)	Tensile strength (MPa)	Carbon Intensity (kg CO_2e/kg of materials)
Hemp fiber	0.86-1.40[43,44]	500-900[43,45]	1.60-4.19[46,47]
Cotton fiber	1.54[48]	496[49]	2.82-3.47[7]
Spider silk fiber	1.34[50,51]	900-1500[51,52]	55[53](synthetic spider silk)
PAN-based carbon fiber	1.75-2.00[54]	3500-7000[55]	22.4-31.0[56,57]
Polyamide fiber (Nylon-6,6)	1.13-1.15[58]	120-304[59,60]	7.30-8.26[7,58]
Polypropylene fiber	0.91-0.92[58]	398-650[61,62]	2.90-3.30[7,58]
Cellulose fiber (Rayon)	0.98-1.00[58]	330-510[58]	3.60-4.00[7,58]
Polyester fiber	1.38[58]	573-1000[58,63]	4.40-5.95[7,58]
Bamboo cellulose macrofiber	1.33-1.57	1580-2220	6.88-8.34

PAN: polyacrylonitrile

Supplementary Table 7 | Tensile strength of fiber-fabric-reinforced epoxy composites.

Species	Matrix	Fiber fraction (%)	Tensile strength (MPa)	Ref.
Jute fiber fabric	Epoxy	-	42.4	[64]
Flax fiber fabric	Epoxy	39.1	127	[65]
Glass/Kevlar hybrid fabric	Epoxy	65.6	341	[66]
Glass fiber fabric	Epoxy	-	330	[67]
Carbon fiber fabric	Epoxy	52	372	[68]
E-glass/Carbon fiber fabric	Epoxy	45	420	[69]
Phenoxy fibre/Carbon fiber fabric	Epoxy	-	520	[70]
Multi-wall carbon nanotubes/Carbon fiber fabric	Epoxy	5	480	[71]
Bamboo cellulose macrofiber fabric	Epoxy	60	350	Our work

Supplementary Video 1. Separation process showing the delignified bamboo stem was separated into thousands of distinct macrofibers.

Supplementary Video 2. The highly oriented bamboo cellulose macrofibers were well retained in water during the separation process.

References

1. Mittal, N. et al. Multiscale control of nanocellulose assembly: transferring remarkable nanoscale fibril mechanics to macroscale fibers. *ACS Nano* **12**, 6378-6388 (2018).
2. Bourmaud, A. et al. Relationships between micro-fibrillar angle, mechanical properties and biochemical composition of flax fibers. *Ind. Crop. Prod.* **44**, 343-351 (2013).
3. Cave, I. D. Theory of X-ray measurement of microfibril angle in wood. *Wood Sci. Technol.* **31**, 225-234 (1997).
4. Park, S. et al. Cellulose crystallinity index: measurement techniques and their impact on interpreting cellulase performance. *Biotechnol Biofuels* **3**, 1-10 (2010).
5. Holzwarth, U. & Gibson, N. The Scherrer equation versus the 'Debye-Scherrer equation'. *Nature Nanotech.* **6**, 534-534 (2011).
6. Howell, C. et al. Effects of hot water extraction and fungal decay on wood crystalline cellulose structure. *Cellulose* **18**, 1179-1190 (2011).
7. Weidema, B. P., et al. Overview and methodology. Data quality guideline for the ecoinvent database version 3. Ecoinvent Report 1(v3). St. Gallen: The ecoinvent Centre (2013).
8. Reutemann, W., & Kieczka, H. Formic acid. Ullmann's encyclopedia of industrial chemistry, (2011).
9. Goor, G., Glenneberg, J., & Jacobi, S. Hydrogen peroxide. Ullmann's encyclopedia of industrial chemistry (2000).
10. AP 42, Fifth Edition, Volume I Chapter 8: Inorganic Chemical Industry. https://www.epa.gov/air-emissions-factors-and-quantification/ap-42-fifth-edition-volume-i-chapter-8-inorganic-chemical-0.
11. Eggeman, T. Sodium hydroxide. Kirk-Othmer Encyclopedia of Chemical Technology, 1-16 (2000).
12. Vogtlander, J. G., & Van der Lugt, P. The environmental impact of industrial bamboo products: Life-cycle assessment and carbon sequestration. *INBAR Technical Report No. 35* (2014).
13. US Department of Transportation, Bureau of Transportation Statistics, Commodity Flow Survey, https://www.bts.gov/cfs. Accessed 03/26/2021.
14. U.S. Life Cycle Inventory Database." National Renewable Energy Laboratory, 2012. https://www.lcacommons.gov/nrel/search. Accessed 01/15/2020.
15. IPCC AR4 Climate Change. The physical science basis: summary for policymakers. Contribution of working group I to the fourth assessment report of the intergovernmental panel on climate change. Cambridge, United Kingdom and New York, USA (2007).
16. Aalde, Harald, et al. Generic methodologies applicable to multiple land-use categories. *IPCC guidelines for national greenhouse gas inventories* **4**, 1-59, (2006).
17. Osorio, L., Trujillo, E., Van, Vuure. W, & Verpoest, I. Morphological aspects and mechanical properties of single bamboo fibers and flexural characterization of bamboo/epoxy composites. *J. Reinf. Plast. Comp.* **30**, 396-408 (2011).
18. Okubo. K., Fujii, T., & Yamamoto, Y. Development of bamboo-based polymer composites and their mechanical properties. *Compos. Part A-Appl. S.* **35**, 377-383 (2004).

19. Phong, N. T., Fujii, T., Chuong, B., & Okubo, K. Study on how to effectively extract bamboo fibers from raw bamboo and wastewater treatment. *J. Mater. Sci. Res*. **1**, 144-155 (2012).
20. Rao, K.M.M., & Rao, K. M. Extraction and tensile properties of natural fibers: Vakka, date and bamboo. *Compos. Struct*, **77**, 288-295 (2007).
21. Wang, X., Yuan, Z., Zhan, X, et al. Multi-scale characterization of the thermal–mechanically isolated bamboo fiber bundles and its potential application on engineered composite. *Constr. Build. Mater*. **262**: 120866 (2020).
22. Kim, H., Okubo, K., Fujii, T., & Takemura, K. Influence of fiber extraction and surface modification on mechanical properties of green composites with bamboo fiber. *J. Adhes. Sci. Technol.* **27**, 1348-1358 (2013).
23. Huang, J. & Young, W. The mechanical, hygral, and interfacial strength of continuous bamboo fiber reinforced epoxy composites. *Compos. Part B-Eng.* **166**, 272-283 (2019).
24. Deshpande, A, Bhaskar, M., & Lakshmana, C. Extraction of bamboo fibers and their use as reinforcement in polymeric composites. *J. Appl. Polym. Sci.* **76**, 83-92 (2000).
25. Mwaikambo, L. Y., & Ansell, M. P. Mechanical properties of alkali treated plant fibres and their potential as reinforcement materials. I. Hemp fibres. *J. Mater. Sci.* **41**, 2483-2496 (2006).
26. Reddy, N., & Yang, Y. Preparation and characterization of long natural cellulose fibers from wheat straw. *J. Agr. Food Chem.* **55**, 8570-8575 (2007).
27. Martinschitz, K. J. et al. Changes in microfibril angle in cyclically deformed dry coir fibers studied by in-situ synchrotron X-ray diffraction. *J. Mater. Sci.* **43**, 350-356 (2008).
28. Beakou, A. et al. Physico-chemical and microstructural characterization of "*Rhectophyllum camerunense*" plant fiber. *Compos. Part A-Appl S*. **39**, 67-74 (2008).
29. Reddy, N., & Yang, Y. Natural cellulose fibers from soybean straw. *Bioresource Technol*. **100**, 3593-3598 (2009).
30. Zhai, S. et al. Tensile strength of windmill palm (*Trachycarpus fortunei*) fiber bundles and its structural implications. *J. Mater. Sci*. 47, 949-959 (2012).
31. Fonseca, A. S. et al. Properties of an Amazonian vegetable fiber as a potential reinforcing material. *Ind. Crop. Prod*, **47**, 43-50 (2013).
32. Saravanakumar, S. S. et al. Characterization of a novel natural cellulosic fiber from *Prosopis juliflora* bark. *Carbohyd Polym*. **92**, 1928-1933 (2013).
33. Wang, R. et al. Tensile properties of single rattan fibers. *Wood Fiber Sci.* **46**, 519-526 (2014).
34. Belouadah, Z., Ati, A., & Rokbi, M. Characterization of new natural cellulosic fiber from *Lygeum spartum L*. *Carbohyd Polym*. **134**, 429-437 (2015).
35. Neto, A. R. S. et al. Comparative study of 12 pineapple leaf fiber varieties for use as mechanical reinforcement in polymer composites. *Ind. Crop. Prod.* **64**, 68-78 (2015).
36. Balaji, A. N., & Nagarajan, K. J. Characterization of alkali treated and untreated new cellulosic fiber from Saharan aloe vera cactus leaves. *Carbohyd Polym*. **174**, 200-208 (2017).
37. Sarasini, F. et al. Biodegradable polycaprolactone-based composites reinforced with ramie

and borassus fibres. *Compos. Struct.* **167**, 20-29 (2017).
38. Chen, Y. et al. Effect of fiber surface treatment on structure, moisture absorption and mechanical properties of luffa sponge fiber bundles. *Ind. Crop. Prod.* **123**, 341-352 (2018).
39. Hyness, N. R. J. et al. Characterization of new natural cellulosic fiber from *heteropogon contortus* plant. *J. Nat. Fibers*. **15**, 146-153 (2018).
40. Vijay, R. et al. Characterization of raw and alkali treated new natural cellulosic fibers from *Tridax procumbens*. *Int. J. Biol. Macromol.* **125**, 99-108 (2019).
41. Manimaran, P. et al. Synthesis and characterization of cellulosic fiber from red banana peduncle as reinforcement for potential applications. *J. Nat. Fibers*. **16**, 768-780. (2019).
42. Reis, R. H. M. et al. *Guaruman* fiber: another possible reinforcement in composites. *J. Mater. Res. Technol.* **9**, 622-628 (2020).
43. Pickering, K. L. et al. Optimising industrial hemp fibre for composites. *Compos. Part A-Appl S.* **38**, 461-468 (2007).
44. Lu, N., & Oza, S. A comparative study of the mechanical properties of hemp fiber with virgin and recycled high density polyethylene matrix. *Compos. Part B-Eng*. **45**, 1651-1656 (2013).
45. Keller, A. Compounding and mechanical properties of biodegradable hemp fibre composites. *Compos. Sci. Technol.* **63**, 1307-1316 (2003).
46. Gonz áez-Garc á, S., Hospido, A., Feijoo, G., & Moreira, M. T. Life cycle assessment of raw materials for non-wood pulp mills: Hemp and flax. *Resour. Conserv. Recy.* **54**, 923-930 (2010).
47. W ötzel, K., Wirth, R., & Flake, M. Life cycle studies on hemp fibre reinforced components and ABS for automotive parts. *Die Angewandte Makromolekulare Chemie*. **272**, 121-127 (1999).
48. Alomayri, T., Shaikh, F. U. A., & Low, I. M. Characterisation of cotton fibre-reinforced geopolymer composites. *Compos. Part B-Eng*. **50**, 1-6 (2013).
49. Kompella, M. K., & Lambros, J. Micromechanical characterization of cellulose fibers. *Polym. Test.* **21**, 523-530 (2002).
50. Pugno, N. M. The “Egg of Columbus” for making the world's toughest fibres. *PLoS One* **9**, e93079 (2014).
51. Griffiths, J. R., & Salanitri, V. R. The strength of spider silk. *J. Mater. Sci.* **15**, 491-496 (1980).
52. Yang, K. et al. Integrating tough *Antheraea pernyi* silk and strong carbon fibres for impact-critical structural composites. *Nat. commun*. **10**, 1-12 (2019).
53. Edlund, A. M., Jones, J., Lewis, R., & Quinn, J. C. Economic feasibility and environmental impact of synthetic spider silk production from escherichia coli. *New Biotechnol*. **42**, 12-18 (2018).
54. Naito, K., Tanaka, Y., Yang, J. M., & Kagawa, Y. Tensile properties of ultrahigh strength PAN-based, ultrahigh modulus pitch-based and high ductility pitch-based carbon fibers. *Carbon* **46**, 189-195 (2008).
55. Chae, H. G. et al. High strength and high modulus carbon fibers. *Carbon* **93**, 81-87 (2015).

56. Das, S. Life cycle assessment of carbon fiber-reinforced polymer composites. *Inter. J. Life Cycle Assess.* **16**, 268-282 (2011).
57. Duflou, J. R. et al. Do fiber-reinforced polymer composites provide environmentally benign alternatives? A life-cycle-assessment-based study. *Mrs Bull*. **37**, 374-382 (2012).
58. Granta Design Limited CES EduPack Software. https://grantadesign.com/education/ces-edupack/(accessed 2020).
59. Baji, A., Mai, Y. W., Wong, S. C., Abtahi, M., & Du, X. Mechanical behavior of self-assembled carbon nanotube reinforced nylon 6, 6 fibers. *Compos. Sci. Technol.* **70**, 1401-1409 (2010).
60. Sanatgar, R. H., Borhani, S., Ravandi, S. A. H., & Gharehaghaji, A. A. The influence of solvent type and polymer concentration on the physical properties of solid state polymerized PA66 nanofiber yarn. *J. Appl. Polym. Sci*. **126**, 1112-1120 (2012).
61. Xue, G., Yilmaz, E., Song, W., & Cao, S. Mechanical, flexural and microstructural properties of cement-tailings matrix composites: effects of fiber type and dosage. *Compos. Part B-Eng*. **172**, 131-142(2019).
62. Wang, D., Ju, Y., Shen, H., & Xu, L. Mechanical properties of high performance concrete reinforced with basalt fiber and polypropylene fiber. *Constr. Build Mater*. **197**, 464-473 (2019).
63. Chae, H. G., & Kumar, S. Rigid–rod polymeric fibers. *J. Appl. Polym. Sci.* **100**, 791–802 (2006).
64. Gujjala, R. et al. Mechanical properties of woven jute–glass hybrid-reinforced epoxy composite. *J. Compos. Mater*. **48**, 3445-3455 (2014).
65. Liu, Q., & Hughes, M. The fracture behaviour and toughness of woven flax fibre reinforced epoxy composites. *Compos. Part A: Appl. Sci. Manufac*. **39**, 1644-1652 (2008).
66. Valença, S. L., Griza, S., de Oliveira, V. G., Sussuchi, E. M., & de Cunha, F. G. C. Evaluation of the mechanical behavior of epoxy composite reinforced with Kevlar plain fabric and glass/Kevlar hybrid fabric. *Compos. Part B: Eng*. **70**, 1-8 (2015).
67. Mahmood, A. H., Gong, R. H., & Porat, I. Improving the bonding strength of laminated composites by optimizing fabric composition. *Polym. Compos*. **33**, 1792-1797 (2012).
68. Karahan, M., & Karahan, N. Investigation of the tensile properties of natural and natural/synthetic hybrid fiber woven fabric composites. *J. Reinf. Plast. Comp*. **34**, 795-806 (2015).
69. Zhang, J., Chaisombat, K., He, S., & Wang, C. H. Hybrid composite laminates reinforced with glass/carbon woven fabrics for lightweight load bearing structures. *Mater. Design* **36**, 75-80 (2012).
70. Wong, D. W., Zhang, H., Bilotti, E., & Peijs, T. Interlaminar toughening of woven fabric carbon/epoxy composite laminates using hybrid aramid/phenoxy interleaves. *Compos. Part A: Appl. Sci. Manufac.* **101**, 151-159 (2017).
71. Rong, H. et al. Comparison of chemical vapor deposition and chemical grafting for improving the mechanical properties of carbon fiber/epoxy composites with multi-wall carbon nanotubes. *J. Mater. Sci.* **48**, 4834-4842 (2013).